Development of Semi-chronic Microdrive System for Large-scale Circuit Mapping in Macaque Mesolimbic and Basal Ganglia Systems*

Shaoyu Qiao, *Member, IEEE*, Kevin A. Brown, Amy L. Orsborn, Breonna Ferrentino, and Bijan Pesaran, *Member, IEEE*

***Abstract*—The development of novel neurotechnologies for treating refractory neuropsychiatric disorders depends on understanding and manipulating the dynamics of neural circuits across large-scale brain networks. The mesolimbic pathway plays an essential role in reward processing and mood regulation and disorders of this pathway underlie many neuropsychiatric disorders. Here, we present the design of a customized semi-chronic microdrive array that precisely targets the anatomical structures of non-human primate (NHP) mesolimbic and basal ganglia systems. We present an integrated experimental paradigm that uses this device to map and manipulate large-scale neural circuits. The system combines electrophysiology, spatiotemporal multisite patterned intracortical microstimulation (ICMS), and diffusion tractography. We propose that this system provides a flexible platform for exploring and identifying neural signatures which can serve as novel targets for closed-loop stimulation in the clinical treatment of neuropsychiatric disorders.**

I. Introduction

Electrical stimulation has been increasingly used as a viable alternative to pharmaceutical medications for treating neuropsychiatric illnesses, such as treatment-resistant depression [1], anxiety [2], and post-traumatic stress disorder [3]. Existing technologies, however, do not offer precise, effective and personalized therapeutic solutions. Neuropsychiatric disorders often impact large-scale brain circuits in interconnected networks. To generate robust and reliable treatments through the identification of appropriate stimulation targets, new neurotechnologies are needed. These technologies can be used to gain a better understanding of how large-scale circuits communicate and how to correct malfunction in these circuits resulting from neurological diseases.

In this paper, we present a semi-chronic microdrive array for large-scale circuit mapping in the mesolimbic and basal ganglia systems of the non-human primate (NHP) brain. We propose an approach to obtaining detailed large-scale functional connectivity mapping by integrating open-loop multisite patterned intracortical microstimulation (ICMS) and diffusion tractography. We illustrate this integrated approach by mapping and manipulating the functional connectivity between the lateral orbitofrontal cortex (lOFC) and the caudate nucleus.

*This work was supported, in part, by the SUBNETS program sponsored by the US Defense Advanced Research Projects Agency (DARPA) Biological Technologies Office (B.P.) and an award from Simons Collaboration on the Global Brain (B.P.).

S. Qiao, K. A. Brown, A. L. Orsborn, B. Ferrentino, and B. Pesaran are with the Center for Neural Science, New York University, NY 10003, USA.

Corresponding author: Bijan Pesaran (phone: 212-998-3578; fax: 212-995-4011; e-mail: bijan@nyu.edu).

II. Large-scale Microdrive System Design

We developed a custom designed large-scale semi-chronic microdrive system for simultaneous intracortical recording and microstimulation for use in large-scale circuit mapping. The design was customized to individual macaque brain, skull and cerebral vasculature (Rogue Research, Montreal) reconstructed using anatomical magnetic resonance images (MRIs) and MRIs using ABLAVAR® contrast agent for angiography with a T1-weighted magnetization-prepared rapid acquisition gradient-echo (MPRAGE) sequence coregistered to the MNI Paxinos labels [4]. The microdrive gives access to relevant structures in the mesolimbic and basal ganglia systems, including OFC, ventral medial prefrontal cortex (vmPFC), anterior cingulate cortex (ACC), thalamus, dorsal and ventral striatum, globus pallidus, and possibly amygdala and hippocampus (Fig. 1).

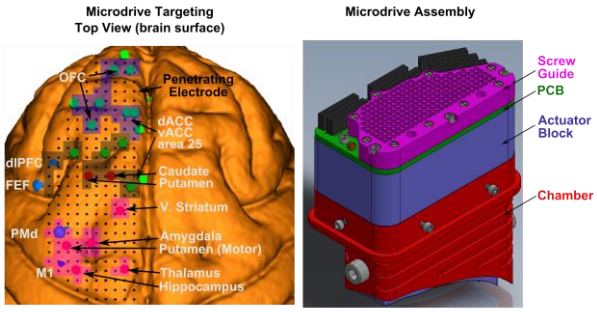

Fig. 1. Left: Anatomical targeting of cortical and subcortical areas of interest on an MRI-based 3-D reconstructed brain. Black dots represent the overlaid electrode grid of the microdrive with 1.5-mm spacing. The color-filled regions represent the three recording banks with ~0.1 MΩ Pt/Ir electrodes targeting all the brain areas of interest. Right: A 3-D drawing of the microdrive assembly where the chamber is made of ultem plastic to maintain MRI compatibility.

The screw-driven actuation mechanism of the microdrive provides bi-directionally independent control of the position of 220 microelectrodes (1.5-mm spacing) along a single axis with a range up to 32 mm with 125-µm pitch [5]. Each actuator consists of a lead screw, a teardrop brass shuttle bonded to the electrode tail with conductive epoxy, and a compression spring. Single electrodes can be moved with an accuracy of approximately 15 µm. Two types of microelectrode were distributed in the microdrive, Platinum/Iridium (Pt/Ir) electrodes (MicroProbes, Gaithersburg, MD) with impedance 0.1–0.5 MΩ for ICMS and intracortical recording, and glass-coated tungsten electrodes (Alpha Omega, Israel) for intracortical recording with impedance 0.8–1.2 MΩ, measured at 1 kHz (Bak Electronics, MD). All anatomical areas of interest in the

mesolimbic and basal ganglia systems can be reached by the Pt/Ir electrodes for ICMS as shown in Fig. 1.

III. Diffusion Weighted Imaging for Precise Anatomical Targeting and Connectivity

We performed multishell high-angular resolution diffusion imaging (HARDI) tractography [6] registered to microdrive implantation. The use of diffusion tractography is essential for developing a rational and individualized approach to stimulating each node in the mesolimbic circuit. Through tractography, we can define each subject's list of stimulation sites and compare possible differences in the results of stimulation due to this form of personalization. Conversely, when a stimulation site is discovered, we can identify long-range anatomical connections to allow more complicated causal perturbations of the circuit.

We collected diffusion weighted images (DWI) to reconstruct white matter tracts linking key cortical and subcortical areas of interest. The animal was anesthetized with isoflurane and placed in the scanner in sphinx position. Data were acquired with a 3-Tesla (3T) Siemens Allegra (Erlangen, Germany) using 3 elements out of a 4-channel phased array from Nova Medical Inc. (Wilmington, MA) and 64 gradient directions in 1.2 mm^2 in-plane resolution (TR = 7000 ms; TE = 110 ms; B-values: 0, 750, 1500, 2250 s/mm^2; FOV: 80×64 pixels; slices: 48; slice thickness: 1.2 mm; DWI to b_0 ratio 65:1).

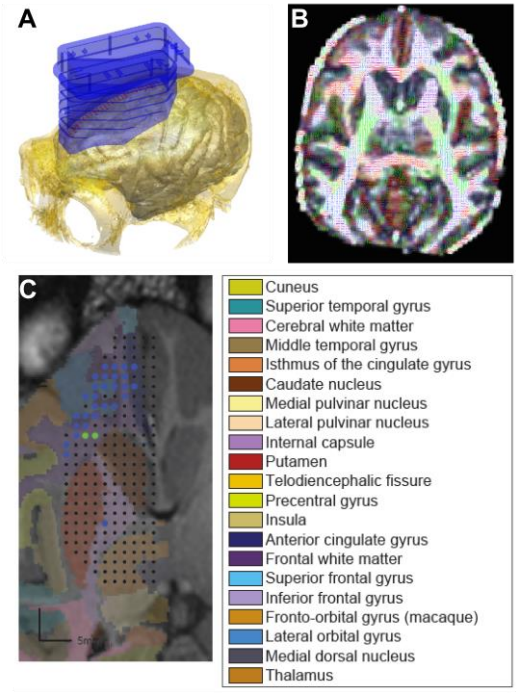

Fig. 2. (A) Brain surface reconstruction of animal implanted with the targeted chamber (in blue). (B) Diffusion weighted inference of local fiber orientation. Overlay: principal axon bundle directions inferred from diffusion weighted imaging vector fields. Each principal diffusion direction vector is red, green, or blue color-coded according to orientation: left-right, anterior-posterior, or dorsal-ventral, respectively. Underlay: anisotropy map shows areas of high (white) and low (gray) diffusivity. High diffusivity indicates major, highly aligned white matter tracts. (C) Anatomical parcellation of white and gray matter structures. Blue dots designate electrodes within 2 mm of transverse slice depth. Green dots show the pair of electrodes for bipolar ICMS. Black dots represent the overlaid microdrive electrode grid.

To correct for geometric distortions from field inhomogeneities caused by the non-zero off-resonance fields, data were collected with reversed phase-encode blips, forming pairs of images with distortions going in opposite directions. From these pairs the susceptibility-induced off-resonance field was estimated using FSL's TOPUP tool [7] and the two images were combined into a single corrected image. Eddy currents generated by the 64 gradient directions were subsequently corrected using FSL's eddy tool [8].

Fig. 2 shows precise coregistration of multishell HARDI to high-resolution anatomical scans, as well as precisely targeted and verified recording locations. Electrodes are advanced in increments of 62.5 µm to 125 µm until they reach anatomical structures of interest. Subsequently, they are finely adjusted, < 62.5 µm, until they touch probable tracts from DWI white matter tractography.

IV. Animal Preparation and Experimental Setup

A. Animal Preparation

All surgical and experimental procedures were conducted in compliance with the National Institute of Health Guide for Care and Use of Laboratory Animals and were approved by the New York University Institutional Animal Care and Use Committee. A male rhesus macaque (*Macaca mulatta*) participated in the study (Monkey M, 8.4 kg). We performed a craniotomy and dura thinning on the targeted area over the left frontal lobe, and implanted a custom-designed large-scale recording chamber (Gray Matter Research, Bozeman, MT) fitted to the skull surface using image-guided stereotaxic surgical techniques (Brainsight®, Rogue Research, Montreal). The chamber was aligned and registered to within 1 mm of the target coordinates (nominally 0.4 mm, 0 degree), and was affixed and sealed to the skull surface via C&B-METABOND® (Parknell Inc.) and dental acrylic. A custom designed large-scale semi-chronic microelectrode microdrive was then inserted into the recording chamber and sealed.

B. Intracortical Recording and Microstimulation

The animal was head-restrained and seated in a primate chair in an unlit sound-attenuated electromagnetically shielded room (ETS Lindgren) with lights switched off. ICMS was applied with a bipolar configuration, made by simultaneously sending a biphasic charge-balanced square wave pulse via a pair of Pt/Ir electrodes with the same pulse amplitude, pulse width, and interphase interval, but opposite polarity (e.g. cathode-lead for electrode 1 and anode-lead for electrode 2) (Cerestim R96, Blackrock Microsystems, Salt Lake City, UT).

Neural recordings during stimulation were made with microelectrodes in the microdrive referenced to a ground screw implanted in the left posterior parietal lobe with the tip of the screw just piercing through the dura mater. Neural signals from all channels were simultaneously amplified and digitized (16 bits at 30 kHz sampling rate; NSpike, Harvard Instrumentation Lab), and continuously streamed to disk during the experiment. We used the stimulus-triggered averaging analysis on the raw broadband neural signals to examine the neural response evoked by ICMS. To suppress the common-mode evoked response, the raw neural response for each channel was locally referenced to its nearest neighbor within 3 mm.

V. Large-scale Circuit Mapping with Patterned Open-loop Intracortical Microstimulation

We sought to assess which nodes in the network displayed inhibitory and excitatory responses due to ICMS pulse trains. We recorded the neural signals from electrodes while stimulating electrodes at other sites. In order to define efficacious open-loop stimulation sites, we focused on functional connectivity mapping of OFC. We used DWI to infer the anatomical connectivity from 1 mm diameter regions to nearby cortical and subcortical recording sites. The scale and precision of our large-scale microdrive allowed iterative re-targeting of electrodes based on a combination of electrophysiological and imaging data. In this paper, we present how we functionally mapped a connection between the lOFC and the body of caudate nucleus using Poisson single-pulse burst stimulation and demonstrate how we manipulated this connection by introducing a high-frequency tetanic stimulation in other brain regions.

A. Circuit Mapping Using Poisson Burst Stimulation

Each Poisson stimulation burst (Fig. 3A) was generated by biphasic charge-balanced square wave pulse trains with pulse amplitude of 50 µA, pulse duration of 100 µs per phase, interphase interval of 53 µs, and pulse frequency of 5 Hz with refractory period of 200 ms. Bipolar stimulation was generated by simultaneously delivering the pulse train via a pair of electrodes with opposite polarity (e.g. cathode-lead: yellow dot; anode-lead: green dot, in Fig. 3D).

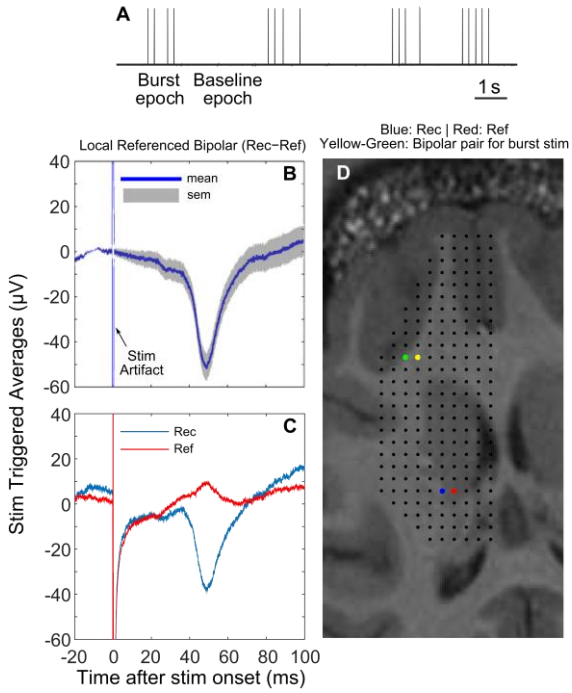

Fig. 3. (A) The Possion burst stimulation sequence consists of 1s pulse bursts with 1-3s baseline periods. (B) The averaged evoked potential (mean ± sem*, n = 497 single-pulse stimulation events) from an electrode (blue dot in D) in the body of caudate nucleus referenced to its neighboring electrode (red dot, in D) resulting from the bipolar burst stimulation from a pair of electrodes (yellow & green dots in D) in the lOFC. (C) The averaged evoked potential from both recording and reference electrodes (blue & red dots in D, respectively) in the body of caudate nucleus. (D) Anatomical MRI at the level where the recording electrode (blue dot) is within 2 mm of transverse slice depth. Black dots are the overlaid electrode grid. *sem represents standard error of the mean.

Fig. 3B shows an example of the averaged bipolar neural response in the body of caudate nucleus evoked by a pair of electrodes stimulating in the lOFC, which was reconstructed by subtracting the evoked response seen from the red electrode from the blue electrode as shown in Fig. 3C. This result suggests that a probable functional connection between the lOFC and the caudate exists.

B. Circuit Mapping Using Spatiotemporal Multisite Patterned Pre-Tetanic-Probe Stimulation

To further test the functional connectivity of the lOFC with caudate, we developed a novel multisite patterned ICMS framework involving 200 Hz tetanic stimulation to investigate how the tetanic stimulation influences the putative lOFC-caudate pathway. As shown in Fig. 4A, the stimulation sequence consists of a pre stimulation from a pair of electrodes to find an excitatory node in the network, a tetanic stimulation from another pair of electrodes in the region with neural responses evoked by the pre stimulation, and a probe stimulation from the same pair of electrodes as the pre stimulation to test excitability of the node.

The pre and probe single pulses were biphasic charge-balanced square waves with amplitude of 30 µA, duration of 100 µs per phase, and interphase interval of 53 µs. The bipolar stimulation was made by simultaneously delivering the pulse via a pair of electrodes with opposite polarity (cathode-lead: yellow dot; anode-lead: green dot, in Fig. 4E). The tetanic stimulation consisted of 50 biphasic charge-balanced square waves with amplitude of 20 µA, duration of 100 µs per phase, and interphase interval of 53 µs.

Fig. 4 shows an example using a pair of electrodes (yellow & green in Fig. 4E) stimulating a node in the lOFC and resulting in an averaged bipolar evoked response in the caudate body (blue & orange in Fig. 4E). The 250-ms tetanic stimulation was delivered through another pair of electrodes (cyan in Fig. 4E) near the responsive electrodes in the caudate body. We observed suppression of both the monopolar (Fig. 4D) and bipolar (Fig. 4B) averaged evoked responses in the caudate body after the tetanic stimulation. This indicates that the functional connection between the lOFC and the caudate was altered by the tetanic stimulation. The putative connection between these two nodes in the network was also confirmed by the DWI tractography as shown in Fig. 4E.

VI. Discussion

Neuropsychiatric disorders are normally reflected in malfunction distributed across multiple regions that are directly and indirectly connected to form a large-scale brain network. Developing a better understanding of these disorders at the network level may lead to novel and improved treatment paradigms. To address this challenge and provide new insights into the mechanisms of large-scale neural circuits, we have presented an experimental platform integrating electrophysiology, ICMS, and diffusion tractography in the NHP. This procedure allows us to flexibly and precisely target and manipulate the circuits in the cortical and subcortical structures of the mesolimbic and basal ganglia systems.

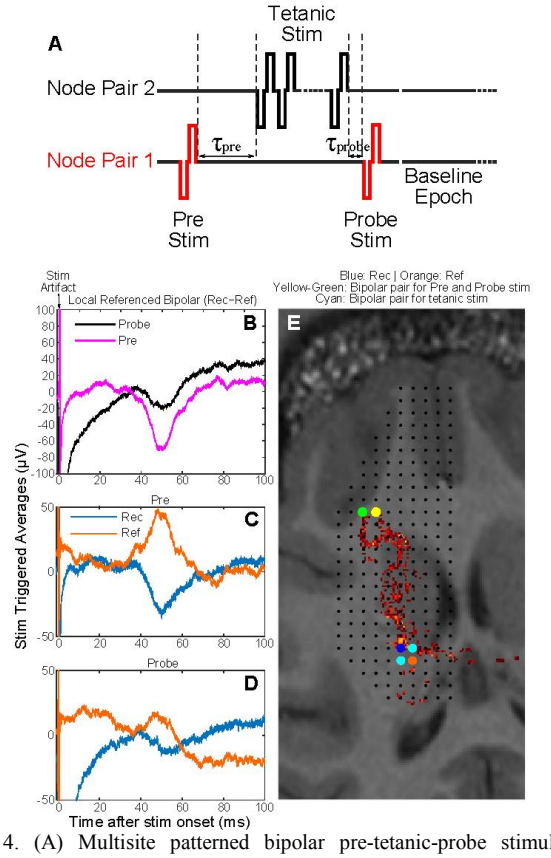

Fig. 4. (A) Multisite patterned bipolar pre-tetanic-probe stimulation framework was implemented via two pairs of electrodes where single-pulse stimulation was delivered via node pair 1 (yellow & green dots in E) before and after tetanic stimulation delivered via node pair 2 (cyan dots in E). (B) The averaged evoked potentials (n = 59 single-pulse stimulation events) for pre and probe stimulations from an electrode (blue dot in E) in the body of caudate nucleus referenced to its neighboring electrode (orange dot, in E) where τ_{pre} = 500 ms and τ_{probe} =20 ms. (C) and (D) The averaged evoked potentials (n = 59) from the recording and reference electrodes (blue & red dots in E, respectively) for pre- and probe stimulation, respectively. (E) Anatomical MRI at the level where the recording electrode (blue dot) is within 2 mm of transverse slice depth, overlaid with the electrode grid (black dots) and a probable tract (red) linking the single-pulse stimulation sites (yellow & green dots) with the recording sites (blue & red dots) estimated via diffusion tractography.

In this paper, we have measured neural responses in the body of caudate nucleus evoked by single-pulse burst microstimulation in the lOFC. We have shown how ICMS can drive excitation across a lOFC–caudate pathway. We have then demonstrated how medium-duration high-frequency tetanic stimulation (250 ms) can drive inactivation blocking the response to excitatory single-pulse stimulation. Further investigation on a clinically-relevant long-duration tetanic stimulation [9] as well as the possible effects of changing latency between the end of the tetanic stimulation and the onset of the probing single-pulse stimulation (τ_{probe}) may help define an effective inactivation protocol to alter processing within the network.

Our spatiotemporal multisite patterned ICMS framework (pre-tetanic-probe) can easily be expanded to include many pre- and probe single-pulse stimulation sites. The framework can also be used to analyze coherence between sites in different brain regions (e.g. OFC, ACC, vmPFC, dorsal and ventral striatum, and globus pallidus) and to assess the network state at different nodes in the large-scale network.

Finally, our system allows us to integrate the proposed multisite patterned ICMS framework into behavior. Combining circuit mapping using ICMS with behavior and neural encoding from the signals during stimulation will provide new insights into how the neuronal dynamics at different nodes of decision-making circuits are modulated in the mesolimbic and basal ganglia systems. Models derived from physiological-functional maps may be used to predict the sites where stimulation will lead to the most effective changes to brain function.

ACKNOWLEDGMENT

We thank Baldwin Goodell for assistance with chamber and microdrive system design. We also thank Ryan Shewcraft, Marsela Rubiano, and C. Octavia Martin for help with animal preparation and experiments, and Keith Sanzenbach and Pablo Velasco for help with magnetic resonance imaging and diffusion weighted imaging.

REFERENCES

[1] D. D. Dougherty, A. R. Rezai, L. L. Carpenter, R. H. Howland, M. T. Bhati, J. P. O'Reardon, E. N. Eskandar, G. H. Baltuch, A. D. Machado, D. Kondziolka, C. Cusin, K. C. Evans, L. H. Price, K. Jacobs, M. Pandya, T. Denko, A. R. Tyrka, T. Brelje, T. Deckersbach, C. Kubu, and D. A. Malone, "A Randomized Sham-Controlled Trial of Deep Brain Stimulation of the Ventral Capsule/Ventral Striatum for Chronic Treatment-Resistant Depression," *Biol. Psychiatry*, vol. 78, no. 4, pp. 240–248, Aug. 2015.

[2] J. M. P. Baas, F. Klumpers, M. H. Mantione, M. Figee, N. C. Vulink, P. R. Schuurman, A. Mazaheri, and D. Denys, "No Impact of Deep Brain Stimulation on Fear-Potentiated Startle in Obsessive-Compulsive Disorder," Front. Behav. Neurosci., vol. 8, Sep. 2014.

[3] J.-P. Langevin, R. J. Koek, H. N. Schwartz, J. W. Y. Chen, D. L. Sultzer, M. A. Mandelkern, A. D. Kulick, and S. E. Krahl, "Deep Brain Stimulation of the Basolateral Amygdala for Treatment-Refractory Posttraumatic Stress Disorder," *Biol. Psychiatry*, Sep. 2015.

[4] S. Frey, D. N. Pandya, M. M. Chakravarty, L. Bailey, M. Petrides, and D. L. Collins, "An MRI based average macaque monkey stereotaxic atlas and space (MNI monkey space)," *NeuroImage*, vol. 55, no. 4, pp. 1435–1442, Apr. 2011.

[5] D. A. Markowitz, Y. T. Wong, C. M. Gray, and B. Pesaran, "Optimizing the Decoding of Movement Goals from Local Field Potentials in Macaque Cortex," *J. Neurosci.*, vol. 31, no. 50, pp. 18412–18422, Dec. 2011.

[6] S. Jbabdi, S. N. Sotiropoulos, A. M. Savio, M. Graña, and T. E. J. Behrens, "Model-based analysis of multishell diffusion MR data for tractography: How to get over fitting problems," *Magn. Reson. Med.*, vol. 68, no. 6, pp. 1846–1855, Dec. 2012.

[7] S. M. Smith, M. Jenkinson, M. W. Woolrich, C. F. Beckmann, T. E. J. Behrens, H. Johansen-Berg, P. R. Bannister, M. De Luca, I. Drobnjak, D. E. Flitney, R. K. Niazy, J. Saunders, J. Vickers, Y. Zhang, N. De Stefano, J. M. Brady, and P. M. Matthews, "Advances in functional and structural MR image analysis and implementation as FSL," *NeuroImage*, vol. 23, pp. S208–S219, Jan. 2004.

[8] J. L. R. Andersson and S. N. Sotiropoulos, "Non-parametric representation and prediction of single- and multi-shell diffusion-weighted MRI data using Gaussian processes," *NeuroImage*, vol. 122, pp. 166–176, Nov. 2015.

[9] C. de Hemptinne, N. C. Swann, J. L. Ostrem, E. S. Ryapolova-Webb, M. San Luciano, N. B. Galifianakis, and P. A. Starr, "Therapeutic deep brain stimulation reduces cortical phase-amplitude coupling in Parkinson's disease," *Nat. Neurosci.*, vol. 18, no. 5, pp. 779–786, Apr. 2015.